Comparison of GPCP Monthly and Daily Precipitation Estimates with High-Latitude Gauge Observations

DAVID T. BOLVIN

Laboratory for Atmospheres, NASA Goddard Space Flight Center, and Science Systems and Applications, Inc., Lanham, Maryland

ROBERT F. ADLER

Laboratory for Atmospheres, NASA Goddard Space Flight Center, Greenbelt, and Earth System Science Interdisciplinary Center, University of Maryland, College Park, College Park, Maryland

GEORGE J. HUFFMAN AND ERIC J. NELKIN

Laboratory for Atmospheres, NASA Goddard Space Flight Center, and Science Systems and Applications, Inc., Lanham, Maryland

JANI P. POUTIAINEN

Finnish Meteorological Institute, Helsinki, Finland

(Manuscript received 4 November 2008, in final form 3 March 2009)

ABSTRACT

Monthly and daily products of the Global Precipitation Climatology Project (GPCP) are evaluated through a comparison with Finnish Meteorological Institute (FMI) gauge observations for the period January 1995–December 2007 to assess the quality of the GPCP estimates at high latitudes. At the monthly scale both the final GPCP combination satellite–gauge (SG) product is evaluated, along with the satellite-only multisatellite (MS) product. The GPCP daily product is scaled to sum to the monthly product, so it implicitly contains monthly-scale gauge influence, although it contains no daily gauge information. As expected, the monthly SG product agrees well with the FMI observations because of the inclusion of limited gauge information. Over the entire analysis period the SG estimates are biased low by 6% when the same wind-loss adjustment is applied to the FMI gauges as is used in the SG analysis. The interannual anomaly correlation is about 0.9. The satellite-only MS product has a lesser, but still reasonably good, interannual correlation (~0.6) while retaining a similar bias due to the use of a climatological bias adjustment. These results indicate the value of using even a few gauges in the analysis and provide an estimate of the correlation error to be expected in the SG analysis over ocean and remote land areas where gauges are absent. The daily GPCP precipitation estimates compare reasonably well at the 1° latitude × 2° longitude scale with the FMI gauge observations in the summer with a correlation of 0.55, but less so in the winter with a correlation of 0.45. Correlations increase somewhat when larger areas and multiday periods are analyzed. The day-to-day occurrence of precipitation is captured fairly well by the GPCP estimates, but the corresponding precipitation event amounts tend to show wide variability. The results of this study indicate that the GPCP monthly and daily fields are useful for meteorological and hydrological studies but that there is significant room for improvement of satellite retrievals and analysis techniques in this region. It is hoped that the research here provides a framework for future high-latitude assessment efforts such as those that will be necessary for the upcoming satellite-based Global Precipitation Measurement (GPM) mission.

Corresponding author address: David T. Bolvin, NASA/GSFC, Code 613.1, Greenbelt, MD 20771.
E-mail: david.t.bolvin@nasa.gov

DOI: 10.1175/2009JAMC2147.1

© 2009 American Meteorological Society

1. Introduction

Knowledge of precipitation is critical to understanding climate variability, including land surface processes and the hydrologic cycle. Precipitation measurements over land typically consist of rain gauge observations that are either automated or require human monitoring. Unfortunately, in geographic areas of sparse population and/or limited resources, or over ocean, quality rain gauge observations with sufficient temporal and spatial coverage are not routinely available. To fulfill the need for globally complete precipitation information, satellite-based estimates using both infrared and microwave sensor data have been developed and are being continually refined. Microwave- and infrared-based precipitation estimates are routinely computed for the tropics and middle latitudes, but these sensors falter over cold surfaces at high latitudes. To fulfill the need for satellite-based precipitation estimates at high latitudes, other satellite data sources must be used. The Global Precipitation Climatology Project (GPCP), version 2 (V2), monthly (Adler et al. 2003) and One-Degree Daily (1DD; Huffman et al. 2001) overcome this limitation at high latitudes (greater than ~50°) through the use of Television Infrared Observation Satellite (TIROS) Operational Vertical Sounder (TOVS) sounding data, with a transition to the Atmospheric Infrared Sounder (AIRS) in April 2005. The TOVS–AIRS estimation technique infers precipitation from clouds using a regression relationship between coincident rain gauge measurements and TOVS–AIRS-based parameters, including cloud-top pressure, fractional cloud cover, and cloud-layer relative humidity (Susskind and Pfaendtner 1989; Susskind et al. 1997).

One crucial aspect of our understanding and improving any satellite-based precipitation estimates is validating the results with high-quality ground-based observations. This validation work serves to show the strengths and weaknesses of the satellite-based estimates, and provides a framework for further improvements of the estimation techniques. Validation of satellite-based estimates, including GPCP, has been performed extensively in the tropics and midlatitudes (Krajewski et al. 2000; Nicholson et al. 2003; McPhee and Margulis 2005; Gebremichael et al. 2005; Dinku et al. 2007). Some large-area validation work has also been performed at high latitudes. Adler et al. (2003) showed that the monthly GPCP V2 satellite–gauge estimates, averaged over the span 1996–98, duplicated well the annual cycle of precipitation as represented by the Baltic Sea Experiment (BALTEX) gauge observations over Sweden. Skomorowski et al. (2001) compared the GPCP 1DD estimates with Mesoscale Alpine Programme (MAP) gauge observations over central alpine Europe for the period June–July 1997 and found the mean correlation was 0.57. Serreze et al. (2005) concluded that the then-current version of the monthly GPCP V2 multisatellite estimates was poorly correlated with dense gauge network observations in the Ob, Yenisey, Lena, and Mackenzie basins for all seasons except summer, for the period 1979–93. Since then, a new version of the multisatellite estimates, described in section 2a, has been introduced making obsolete the dataset used in Serreze et al. (2005). Analysis results using the new corrected GPCP V2 multisatellite estimates are presented in this paper.

Continued analysis of high-latitude precipitation is important, as estimating satellite-based precipitation at latitudes greater than 60° currently presents a major challenge in computing global rainfall products. Neither microwave nor infrared estimates can differentiate between cold or icy surface and frozen precipitation. Furthermore, infrared brightness temperatures cannot discriminate precipitation in stratiform clouds that are typical at high latitudes. Though the GPCP datasets, using primarily TOVS or AIRS data (hereafter referred to as TOVS–AIRS data), provide reasonable estimates of precipitation at high latitudes, their accuracy must be determined through careful comparison with ground-based observations.

Historically, it has been difficult to access high-quality ground-based precipitation estimates covering the high-latitude regions for research purposes, making validation efforts challenging. To assist in these efforts, we used the Finnish Meteorological Institute (FMI) gauge dataset, which consists of a long record of quality-controlled, high-density rain gauge observations that measure both liquid and solid (liquid equivalent) precipitation. Geographically and temporally, the FMI gauge dataset overlaps with the Helsinki test bed mesoscale observation network, which will be used for future satellite observation assessment activities. The spatial density of the FMI observations provides an excellent opportunity for comparison with and assessment of the GPCP estimates at the grid-box monthly and daily scales. The goal is to quantify the nature of the differences at the high latitudes to further understand the small-scale errors associated with the satellite-based GPCP estimates and provide a framework for future improvements to the estimation techniques. This framework can also serve as the basis for routine comparison and validation of high-latitude precipitation estimates from future missions such as the Global Precipitation Measurement (GPM) mission.

This paper describes the results of the comparison between the GPCP monthly–daily estimates and the FMI gauge observations. The GPCP and FMI datasets are described in section 2, and the analysis methodology

is outlined in section 3. Section 4 provides the comparison results, and section 5 presents the conclusions.

2. Datasets

Descriptions of the GPCP and FMI datasets, used in this analysis, are provided in the following sections. Since this analysis exclusively covers latitudes greater than 60°N, only the input data and merging techniques for the GPCP monthly and daily products at the high latitudes will be detailed here. Similarly, only the input datasets and merging techniques for the analysis span, January 1995–December 2007, will be discussed. For details on all the input sources and complete GPCP monthly and daily global merger processes, see Adler et al. (2003) and Huffman et al. (2001), respectively.

a. GPCP monthly estimates

The GPCP, an international activity of the Global Energy and Water Experiment (GEWEX), was implemented with the task of developing and producing long-term, global precipitation analyses at monthly and finer time scales. The monthly product is global, has a spatial resolution of 2.5° latitude × 2.5° longitude, and is available for the span January 1979–(delayed) present. The complete monthly dataset consists of 27 precipitation and precipitation-related products, but this current analysis will focus on the multisatellite (MS) and the satellite–gauge (SG) precipitation estimates. The Global Precipitation Climatology Centre (GPCC) gauge analyses (Rudolf 1993, 1996; Rudolf et al. 1994), which are an input to the SG product, will also be examined in the analysis.

For the current analysis span, and for the latitudes of interest in this analysis (>60°N), the MS product is computed for each month based primarily on scaled TOVS and AIRS precipitation estimates. The TOVS estimates span the period up to and including March 2005, with AIRS starting in April 2005 and continuing to the present. The TOVS–AIRS algorithm uses an atmospheric model (or climatology) to generate a first guess for the retrieval of various atmospheric parameters, including cloud-top pressure, fractional cloud cover, and the relative humidity profile from National Oceanic and Atmospheric Administration (NOAA) series satellite data. The precipitation algorithm is a regression between these parameters and surface data stratified by latitude, month, and land–ocean surface type (Susskind and Pfaendtner 1989; Susskind et al. 1997). The statistical (empirical) nature of the TOVS–AIRS estimates suggests they are of lesser quality than corresponding physically based Special Sensor Microwave Imager (SSM/I) microwave estimates, but are still sufficiently accurate and useful to include in precipitation combinations where present-generation high-latitude microwave estimates are unusable.

The TOVS–AIRS estimates are not used as is, but rather are scaled to higher-quality SSM/I microwave estimates in the midlatitudes and GPCC gauge estimates at the polar latitudes. The goal is to have a spatially coherent and homogeneous precipitation field that has the presumably lower bias of the SSM/I estimates and the GPCC gauge analyses. To draw on their perceived strengths, the SSM/I and TOVS–AIRS estimates, and GPCC gauge analyses, are composited to form the "preliminary" MS estimate (Adler et al. 2003). The result is a smoothly varying, spatially coherent preliminary MS precipitation field that has the large-scale bias of the SSM/I estimates in the midlatitudes and large-scale bias of the GPCC gauge analysis in the northerly polar region, with the bulk of the adjusted estimates coming from TOVS–AIRS. After being used to compute the SG, the preliminary MS field is then adjusted to the large-scale monthly climatological bias of the SG to form the "final" MS estimate. The net effect of this last step is to add a large-scale climatological (i.e., not varying from year to year) gauge adjustment to the MS over land. This adjustment to the preliminary MS was instituted for ongoing processing in July 2006, and applied retroactively to all previous MS estimates as noted above. Throughout the remainder of this paper, the final MS estimates will be referred to as MS.

The SG product is produced by first adjusting the preliminary MS estimate to the large-scale monthly GPCC gauge average for each grid box over land. Then, the gauge-adjusted preliminary MS estimate and the GPCC gauge analysis are combined into a weighted average, where the weights are the inverse (estimated) error variance of the respective estimates. It is important to note that the Legates (1987) climatological wind-loss bias correction is applied to the GPCC gauge analyses prior to combination with the preliminary MS estimate. This wind-loss correction raises the estimated GPCC gauge analysis amounts by approximately 5%–400%, depending on the assumed typical gauge type, surface wind speed, and precipitation fall speed. Gauge undercatch (and therefore wind-loss adjustment) is higher for frozen precipitation than for liquid precipitation. Furthermore, wind speed is the most important environmental factor contributing to the systematic undermeasurement of solid precipitation by gauges (Goodison et al. 1998). As a result, the wind-loss adjustment is largest at high latitudes and lowest in the tropics. Throughout the remainder of this paper, SG estimates will be referred to as SG.

Examples of the SG for February 2007 and August 2007, centered on Finland, are shown in Figs. 1a and 1b, respectively. February shows relatively light precipitation over Finland and the surrounding areas compared to August. Most noticeable in February is the low pressure system off the west coast of Norway, where strong land–sea temperature gradients and complex terrain contribute significantly to enhanced precipitation. This effect is seen to a much lesser extent in August.

b. GPCP daily estimates

The GPCP responded to user-community requirements for finer-scale precipitation data by commissioning production of the daily product, which has a daily temporal and 1° spatial resolution, hence the name One-Degree Daily (1DD). The data spans the period from October 1996 to the (delayed) present, with the GPCP day being defined as 0000–0000 UTC. As in the GPCP monthly product, scaled TOVS–AIRS estimates are the primary data source at high latitudes. Because of the higher temporal resolution, the scaling–merging procedure for the TOVS–AIRS must be retailored to suit the 1DD resolution. We briefly describe the threshold–match precipitation index (TMPI) estimates that make up the 1DD in the latitude band 40°N–40°S and form a boundary condition for the high-latitude precipitation estimates. The TMPI uses SSM/I precipitation estimates, geosynchronous IR (geo-IR) and low-earth-orbit IR (leo-IR) brightness temperatures, and the (monthly) SG product to estimate the daily precipitation. The TMPI is similar to the Geostationary Operational Environmental Satellite (GOES) precipitation index (GPI), but with the rain–no-rain threshold in brightness temperature set locally in space and time using the SSM/I to constrain the fractional occurrence of precipitation, and a single (local) conditional rain rate based on the (monthly) SG product to set the rain amount (Huffman et al. 2001). This ensures consistency between the GPCP monthly and daily products, and also has the beneficial effect of implicitly including wind-loss-adjusted gauge "influence" into the GPCP daily product.

A time series of GPCP daily images for the period 15–18 February 2007 is shown in Figs. 2a–d. On 15 February, precipitation from a series of typical wintertime frontal systems can be seen. Most noticeable is the strong low pressure system south of Iceland and west of Great Britain. On 16 February, the cold front associated with this strong low is clearly visible, moving eastward and extending from the east coast of Greenland to the west coast of France and beyond. A warm front, associated with and preceding this cold front, has produced precipitation over the bulk of Finland. By 17 February, the low pressure system has weakened considerably while

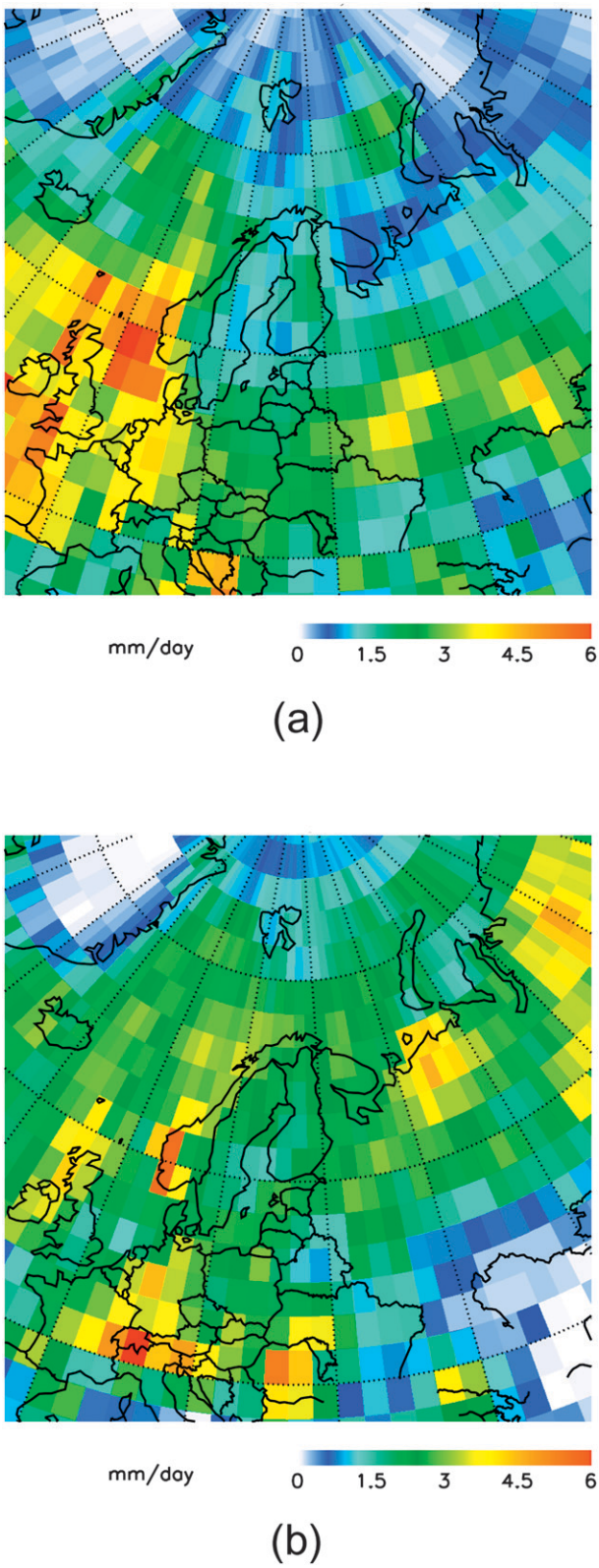

FIG. 1. GPCP monthly SG precipitation estimates (mm day^{-1}) for an area centered around Finland for (a) February and (b) August 2007.

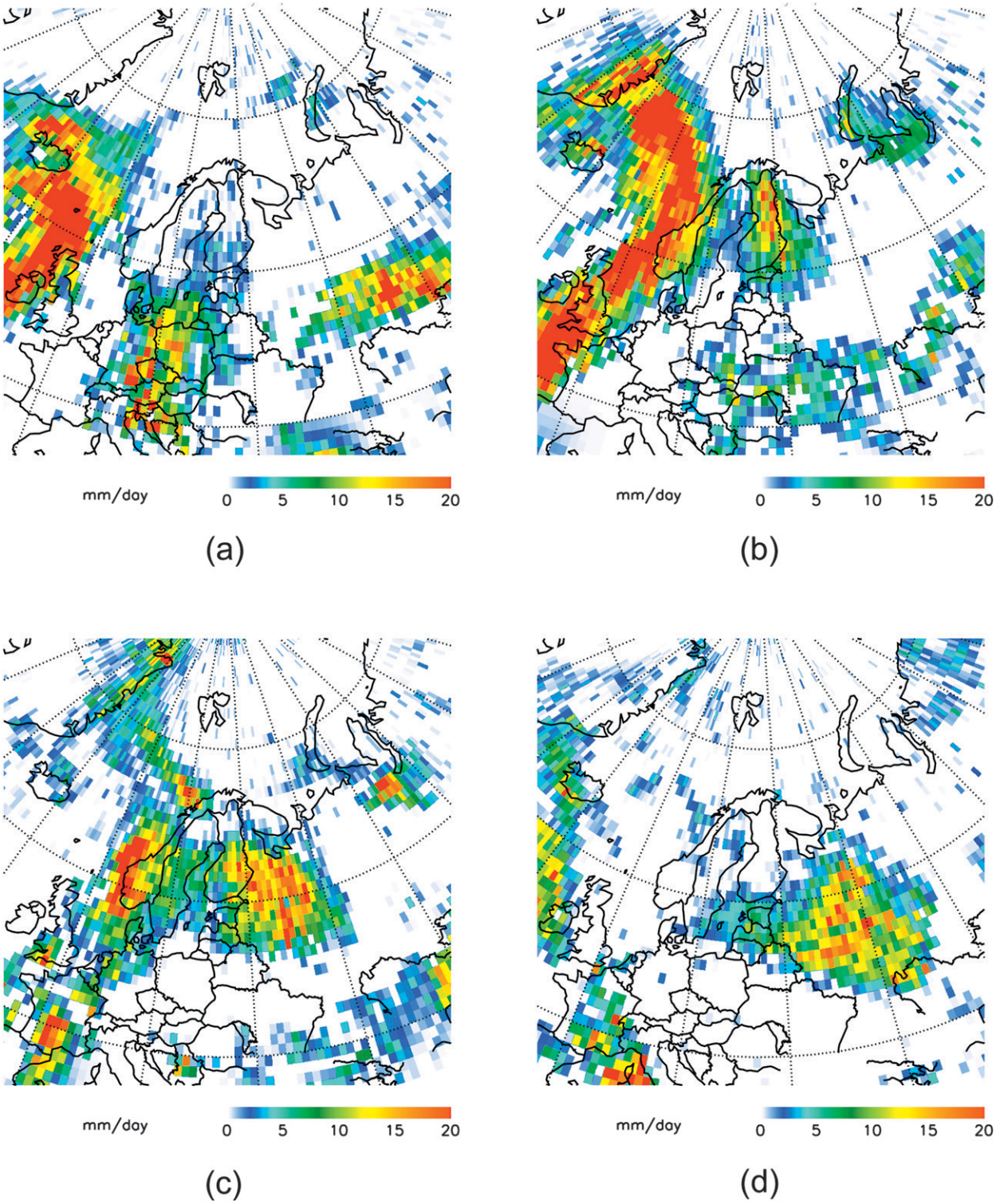

FIG. 2. GPCP daily precipitation estimates (mm day^{-1}) for an area centered around Finland for (a)–(d) 15–18 Feb 2007.

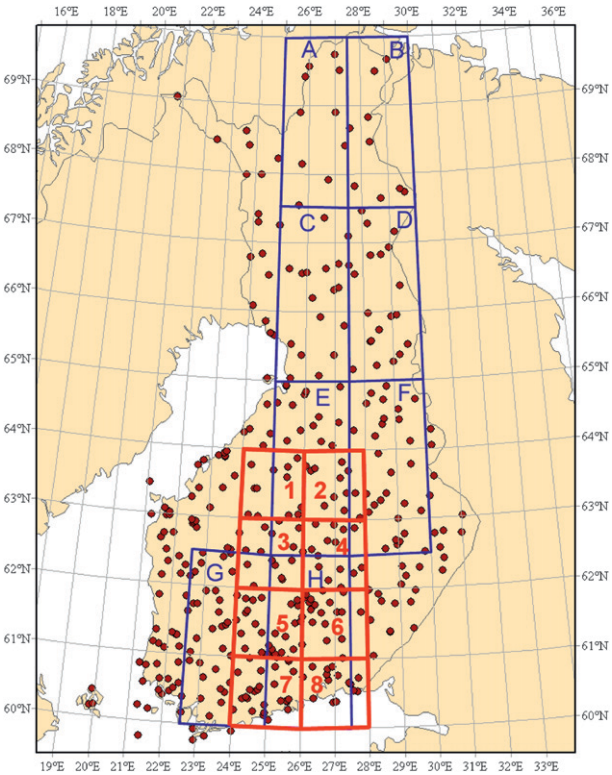

FIG. 3. Example distribution of FMI gauges (red dots) over the analysis span January 1995–December 2007. Boxes A–H (blue) show the geographical area used in the 2.5° monthly analysis and boxes 1–8 (red) show the geographical area used in the 1° latitude × 2° longitude daily analysis.

the preceding warm front continues to propagate eastward and produce precipitation over western Russia. On 18 February, the low has dissipated but the warm front still continues to produce precipitation over western Russia. The leading edge of the next low pressure system is seen south of Iceland.

c. *FMI gauge observations*

The FMI gauge observation network consists of approximately 400 reporting stations during the current period of analysis, January 1995–December 2007. The typical geographic distribution of these stations is shown in Fig. 3. In general, the gauge population is denser in southern Finland and becomes progressively sparser moving northward. The number of gauges was consistent throughout the entire analysis period with an insignificant number of station reporting gaps. In this dataset, the vast majority of the observations was taken using the manual Finnish H&H-90 bucket gauge with Tretyakov wind shielding. However, approximately 30 of these manual gauges were replaced during the 2004–07 period with automated weighing gauges (also with Tretyakov wind shielding). According to the FMI, the changeover from manual to automated gauges is not expected to affect the homogeneity of the data record. All observations are reported as daily accumulations from 0600 to 0600 UTC, and measure both liquid and solid (as liquid equivalent) precipitation. To determine the liquid equivalent, frozen precipitation is accumulated and manually melted, except at automated stations where antifreezing liquid is used in the bucket. All gauge observations are subjected to standard and routine quality control, but no wind-loss adjustment is applied to the observations. The excellent quality, long homogenous record, spatial density, ability to measure frozen precipitation, and availability of the FMI gauge observations make them ideal candidates for comparison with grid-box-level satellite-based precipitation estimates. The details of the FMI station data can be found in Drebs et al. (2002). It is important to note that the 0600–0600 UTC FMI "day" is shifted 6 h from the 0000–0000 UTC GPCP 1DD day. This offset will be considered when interpreting the daily results in section 4b.

3. Analysis methodology

The GPCP monthly and daily precipitation results are compared to the FMI gauge precipitation at several different spatial scales. As the GPCP precipitation estimates are gridded, the FMI gauge observations must also be gridded to the same scales for consistency. For the GPCP monthly product, which has a native 2.5° latitude × 2.5° longitude spatial resolution, all the FMI observations that lie in the corresponding 2.5° latitude × 2.5° longitude grid boxes for the month are equal-weighting averaged to form a single FMI precipitation observation. This relatively simple scheme was deemed sufficient for computing the grid-box average given the very high density of the FMI gauge population.

At the daily scale, it was deemed preferable to average both the GPCP daily estimates and the FMI observations to a 1° latitude × 2° longitude grid to obtain approximately square grid boxes (at the latitudes of Finland), which are commonly used in hydrological analyses. When gridding gauge observations to relatively small spatial scales, the possible uneven distribution of the gauges in a given grid box can lead to a geographical bias in the average. We mitigated this possibility by first gridding the FMI observations to 0.25° latitude × 0.5° longitude resolution with equal-weighting averaging. Then, the eight 0.25° latitude × 0.5° longitude grid-box averages were then equal-weighting averaged to form the 1° latitude × 2° longitude grid-box average. As for the 2.5° latitude × 2.5° longitude spatial resolution, the FMI gauge population was deemed sufficiently dense such that an equal-weighting

TABLE 1. Average number of FMI and GPCC gauges over the analysis span January 1995–December 2007 for each of the eight blue 2.5° grid boxes A–H in Fig. 3.

Box	Avg no. of FMI gauges	Avg no. of GPCC gauges
A	12	2
B	9	1
C	16	3
D	22	2
E	42	2
F	34	4
G	63	5
H	67	6

averaging technique would produce a representative areal average.

To give a sense of the FMI gauge density over the analysis area for the GPCP monthly product, the gauge population varies from 9 to 67 gauges per grid box at 2.5° resolution, with 33 being the average number of gauges per 2.5° grid box. Over the GPCP daily analysis area, the gauge population varies from 13 to 25 gauges per grid box at 1° latitude × 2° longitude resolution, with 18 being the average number of gauges per 1° latitude × 2° longitude grid box. The details of the geographic areas studied, in addition to the relative GPCC and FMI gauge populations, for the GPCP monthly and daily analyses are provided in section 4.

Since the FMI gauge observations are used in this analysis as the benchmark for comparing with the GPCP estimates, it is relevant to consider the errors inherent in the FMI grid-box averages. Rudolf and Schneider (2005) showed that the relative error levels for 25 gauges in a 2.5° latitude × 2.5° longitude grid box on the monthly time scale are approximately 3% and 6% in the winter and summer, respectively. These results were based on analysis of dense gauge networks in Australia, Canada, Finland, Germany, and the United States. Considering there are, on average, 33 FMI gauges in a 2.5° latitude × 2.5° longitude grid box, the relative error will be smaller.

The results of the comparisons between the monthly GPCP estimates and the FMI observations and the daily GPCP estimates and the FMI observations are presented in sections 4a and 4b, respectively.

4. Comparison results

a. Monthly product

The goal of the monthly product comparisons is to assess the long-term, large-area biases and correlations between the GPCP monthly estimates and FMI observations. Figure 3 shows the eight 2.5° grid boxes (blue boxes A–H) used in the large-area monthly product comparisons. These boxes each contain a reasonable distribution of FMI gauges and minimal (ungauged) ocean surface. For reference, the average number of FMI and GPCC gauges for each of the eight 2.5° grid boxes over the analysis span is shown in Table 1.

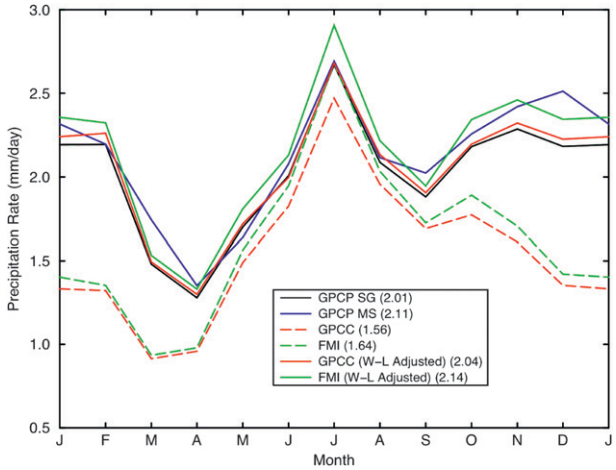

FIG. 4. Time series of monthly climatological averages of the SG estimates (solid black), MS estimates (solid blue), wind-loss-adjusted and -unadjusted GPCC analyses (solid and dashed red, respectively), and wind-loss-adjusted and -unadjusted FMI observations (solid and dashed green, respectively), averaged over the 13-yr span January 1995–December 2007 and over the eight 2.5° grid boxes. The annual average of each product (mm day^{-1}) is provided in the legend. January is duplicated after December for visual continuity.

Figure 4 shows the monthly climatological averages of the SG, MS, wind-loss adjusted and unadjusted GPCC analyses, and wind-loss adjusted and unadjusted FMI observations, averaged over the 13-yr span January 1995–December 2007 and over the eight 2.5° grid boxes. The annual average of each product (in mm day^{-1}) is provided in the Fig. 4 legend. Note that January is duplicated after December for visual continuity. The seasonal cycle of precipitation is consistently captured by all six products, with the average precipitation rates reaching a peak in the summer and a minimum in the spring. As expected, the SG (2.01 mm day^{-1}) and wind-loss-adjusted GPCC (2.04 mm day^{-1}) averages are nearly identical since the wind-loss-adjusted GPCC estimates dominate the SG over land. The unadjusted GPCC (1.56 mm day^{-1}) and FMI (1.64 mm day^{-1}) agree well in winter and spring but slightly less so in summer and fall, with the FMI being consistently higher for all months. This offset between the GPCC and FMI may be due to a number of factors. The GPCC analysis, which is

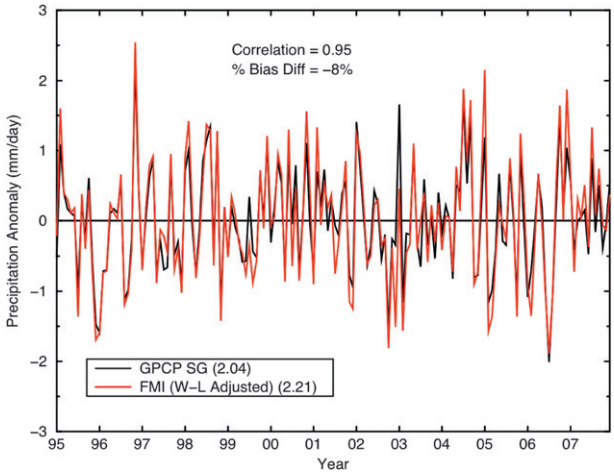

FIG. 5. Time series of monthly SG (black) and wind-loss-adjusted FMI (red) precipitation anomalies for 2.5° grid box E over the entire analysis span January 1995–December 2007. The annual average of both products (mm day^{-1}) is provided in the legend.

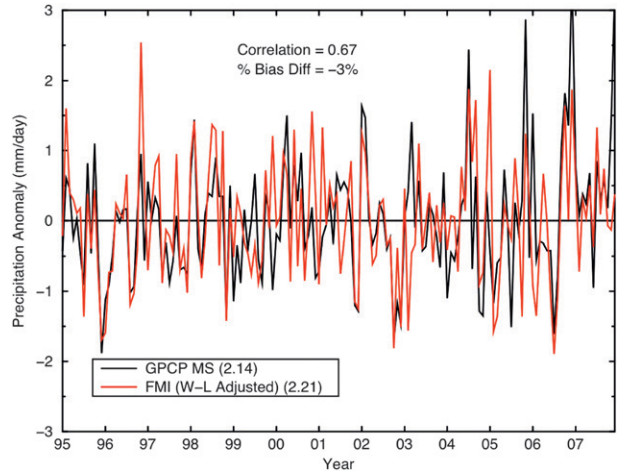

FIG. 6. As in Fig. 5, but for time series of monthly MS (black) and wind-loss-adjusted FMI (red) precipitation anomalies.

based on a subset of FMI gauges over Finland, contains far fewer gauges in a 2.5° grid box compared to the (complete) FMI gauge distribution as shown in Table 1. It is possible that the analysis technique used by GPCC, which uses fewer gauges and relies on the gauge influence from the surrounding grid boxes, tends to bias the resulting precipitation amounts low. Although it is true that in areas of complex terrain the GPCC analysis tends to underestimate precipitation, the effect is likely not important as Finland's topography is relatively flat south of 67°N.

Because the Legates wind-loss adjustment is a single-grid-box multiplicative factor, the wind-loss-adjusted GPCC (2.04 mm day^{-1}) and FMI (2.14 mm day^{-1}) show the same level of correlation as the unadjusted GPCC and FMI. As evidenced by the difference between the wind-loss-adjusted and unadjusted GPCC (and FMI) results, the wind-loss adjustment follows a predictable seasonal cycle: largest in the winter and smallest in the summer. The MS (2.11 mm day^{-1}), which is based solely on scaled TOVS–AIRS estimates at higher latitudes, agrees well with the SG in the summer but less so in fall and winter.

The next step in the analysis is to examine how the GPCP monthly products and the FMI compare at smaller spatial scales. To show skill at smaller spatial scales, the GPCP products must be able to duplicate the interannual variability of the FMI precipitation. This is evaluated by examining the 13-yr time series of monthly precipitation anomalies for the SG and the FMI for grid box E (see Fig. 3). Grid box E was selected as it contains a representative FMI gauge population and is centrally located in the study area. The 12 monthly climatologies for the SG and FMI are computed using all 13 yr of data, and the monthly SG and FMI anomalies are computed from their corresponding climatologies. The time series of SG and wind-loss-adjusted FMI precipitation anomalies is shown in Fig. 5. The annual average of both products (in mm day^{-1}) is provided in the Fig. 5 legend. The interannual variations in the FMI are duplicated remarkably well by the SG, showing an anomaly correlation of 0.95 over the analysis period. This high anomaly correlation indicates the value of incorporating the GPCC gauge analysis into the SG, even though that analysis is based on a relatively small number of gauges in a 2.5° grid box. The standard deviation of the anomalies in Fig. 5 is 0.75 mm day^{-1} for the SG and 0.88 mm day^{-1} for the FMI. To assess the long-term bias of the SG relative to the FMI, the percent bias difference is defined as

$$\%\text{Bias Diff} = [(\text{GPCP} - \text{FMI}_{\text{WLA}})/\text{FMI}_{\text{WLA}}] \times 100,$$

TABLE 2. Anomaly correlation coefficient and percent bias difference between the monthly SG estimates and wind-loss-adjusted FMI gauge observations for each of the eight blue 2.5° grid boxes A–H in Fig. 3.

Box	Anomaly correlation coef	Bias diff (%)
A	0.96	−3
B	0.90	−6
C	0.94	−6
D	0.95	−3
E	0.95	−8
F	0.97	−13
G	0.99	−5
H	0.97	−0.5

TABLE 3. Anomaly correlation coefficient and percent bias difference between the monthly MS estimates and wind-loss-adjusted FMI gauge observations for each of the eight blue 2.5° grid boxes A–H in Fig. 3.

Box	Anomaly correlation coef	Bias diff (%)
A	0.56	1
B	0.54	−0.4
C	0.53	−3
D	0.62	0.2
E	0.67	−3
F	0.67	−6
G	0.77	−4
H	0.68	6

where GPCP is the average of all the monthly GPCP (SG in this case) estimates and FMI_{WLA} is the average of all the wind-loss-adjusted FMI observations in the analysis span. On average, the SG is biased low by 8% compared to the wind-loss-adjusted FMI for grid box E, which is consistent with the large-area results shown in Fig. 4.

Figure 6 shows the time series of monthly anomalies for the MS product and the wind-loss-adjusted FMI for grid box E. The annual average of both products (in mm day^{-1}) is provided in the Fig. 6 legend. The MS anomalies are not as well correlated with the wind-loss-adjusted FMI as the SG, but are still reasonable at 0.67. The standard deviation of the anomalies in Fig. 6 is 0.90 mm day^{-1} for the MS and 0.88 mm day^{-1} for the FMI. The MS product is biased low by 3% for grid box E, which is also consistent with the results shown in Fig. 4. The expected small bias, similar in magnitude to that of the SG product, is due to the climatological (by month) adjustment of the satellite estimates. The 0.67 anomaly correlation indicates that the satellite-only information is capturing much of the actual interannual variation over this grid.

As seen in Fig. 5, the interannual anomaly correlation between the SG and the wind-loss-adjusted FMI for grid box E is 0.95 while the percent bias difference is −8%. Table 2 shows the corresponding statistics for all eight 2.5° grid boxes (A–H). The anomaly correlations are high and vary from 0.90 to 0.99. The SG product is consistently biased low with respect to the wind-loss-adjusted FMI observations, ranging from −0.5% to −13%. These statistics are striking considering the differences between the grid-box GPCC and FMI gauge populations as shown in Table 1. It is not apparent that the number of gauges in either the GPCC or FMI affects the percent bias differences or anomaly correlations. It is important to note that the gauges used in the GPCC analysis are a small subset of the FMI gauge dataset, and that the GPCC and FMI gauge complements do fluctuate over the analysis span but not to a level believed to significantly affect the results. It is also important to understand that the GPCC analysis technique (Shepard 1968; Willmott et al. 1985) does ''reach out'' to neighboring grid boxes, so gauge observations in adjacent grid boxes do have some influence on the final result.

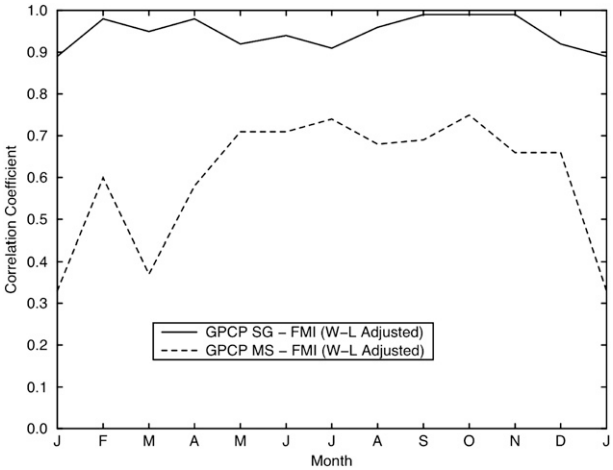

FIG. 7. Time series of monthly climatological anomaly correlation coefficients between the monthly SG estimates and the wind-loss-adjusted FMI gauge observations (solid line), and the monthly MS estimates and wind-loss-adjusted FMI gauge observations (dashed line), for 2.5° grid box E. January is duplicated after December for visual continuity.

Table 3 shows the percent bias differences and anomaly correlations between the MS and wind-loss-adjusted FMI for all eight 2.5° grid boxes (A–H). The MS product does not capture the month-to-month anomalies as well as the SG, but the correlations are still reasonable, ranging from 0.53 to 0.77. The percent bias differences range from −6% to 6%, underscoring the nature of the monthly climatological SG bias adjustment. Interestingly, the range of percent bias differences is approximately the same for the SG and MS products at about 12%. However, the MS product percent bias differences tend to be centered around zero. This is somewhat surprising, as one would expect the monthly GPCC gauge analysis in the SG would provide a truer representation of the precipitation than a monthly climatological SG adjustment in the MS. It is possible that this adjustment is somehow boosting the precipitation rates by a small margin at the latitudes of this analysis, contributing to the perceived smaller bias in the MS when compared with the FMI. Further investigation into the monthly climatological SG adjustment at the higher latitudes may be warranted to fully understand these differences. The results shown in Fig. 6 and Table 3 are in stark contrast to the results found in Serreze et al. (2005), who showed zero correlation between the MS and gauge over

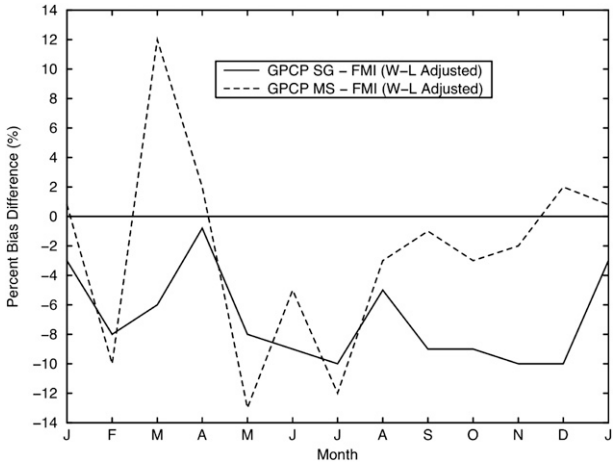

FIG. 8. Time series of the monthly climatological percent bias difference between the monthly SG estimates and the wind-loss-adjusted FMI gauge observations (solid line), and the monthly MS estimates and wind-loss-adjusted FMI gauge observations (dashed line), for 2.5° grid box E. January is duplicated after December for visual continuity.

four large-area basins. As noted above, the MS dataset available to Serreze et al. (2005), equivalent to the present preliminary MS (defined in section 2a), lacked the consistency that the climatological adjustment now produces in the present final MS. Accordingly, it is not surprising that the results here differ significantly from theirs.

Figures 5 and 6 showed the anomaly correlation and percent bias difference between the SG and wind-loss-adjusted FMI, and the MS and wind-loss-adjusted FMI, respectively, for 2.5° grid box E for all months in the analysis span. To determine how the anomaly correlations and percent bias differences vary monthly or seasonally throughout the annual cycle, the SG, MS, and wind-loss-adjusted FMI monthly averages were computed and composited by month of year for the grid box E. The climatological anomaly correlations for each month between the SG and the wind-loss-adjusted FMI, and the MS and wind-loss-adjusted FMI, are shown in Fig. 7. Note that January is duplicated after December for visual continuity. There appears to be no monthly or seasonal bias in the SG anomaly correlations, which are 0.90 or larger. The MS anomaly correlations are lower for all months, and tend to be lowest in the winter and spring and highest in the summer and fall. Other 2.5° grid boxes also show consistently high SG anomaly correlations throughout the year, with no discernable annual cycle and a lower bound of 0.90. The MS anomaly correlations tend to be low in the winter and spring but exhibit high variability from grid box to grid box. Overall, the summer and fall anomaly correlations tend to be higher, with minimal grid-box to grid-box variation. This leads to the conclusion that the GPCP high-latitude satellite sources, TOVS or AIRS, or techniques perform worse in the winter and spring than summer and fall.

Figure 8 shows the monthly climatological percent bias differences between the SG and the wind-loss-adjusted FMI, and the MS and the wind-loss-adjusted FMI for grid box E. The SG differences are consistently (small) negative throughout the annual cycle while the MS differences are both positive and negative, and exhibit larger variability. The MS differences are large positive in March and April, large negative in late spring/early summer, and tend to zero in the fall and early winter. Examination of other 2.5° grid boxes shows that the SG percent bias differences are consistently negative throughout the year. The MS percent bias differences show much larger grid-box to grid-box variability, though generally the large positive differences are still seen in March and April, and the large negative differences are seen in late spring/early summer. The high variability is likely due to the nature of the climatological SG bias adjustment, which consists of a fixed set of 12 monthly, spatially varying multiplicative ratio fields.

The monthly GPCP MS and SG product analysis results over Finland indicate that the SG is superior to the MS even in areas of low gauge coverage and should be the product of choice for the study of any interannual (or longer) variations. In areas largely lacking gauge coverage, such as oceanic regions and remote land areas, the SG is equivalent to the MS, so the MS results shown here should provide a lower bound of SG quality in such regions in terms of interannual correlations.

b. *Daily product*

The goal of the daily product comparisons is to quantify the relationship between the GPCP estimates and FMI observations at smaller spatial and temporal scales, and to assess the skill of the GPCP estimates in capturing day-to-day precipitation events as reflected in the FMI observations. For consistency, the FMI gauge observations and GPCP daily estimates are gridded to the same 1° latitude × 2° longitude resolution as described in section 3. Figure 3 shows the eight 1° latitude × 2° longitude grid boxes (red boxes 1–8) used in the daily product comparisons. In parallel with the blue 2.5° grid boxes, this area was selected as it contains a homogeneous distribution of FMI gauges and minimizes the amount of sea surface. The daily analysis will focus on two months, August 2005 and February 2006, which provide a representative summer and winter month, respectively.

Figure 9a shows a scatterplot of the daily GPCP versus FMI for all 1° latitude × 2° longitude grid box precipitation estimates from boxes 1–8 for August 2005. The daily GPCP estimates are well correlated at 0.60, but

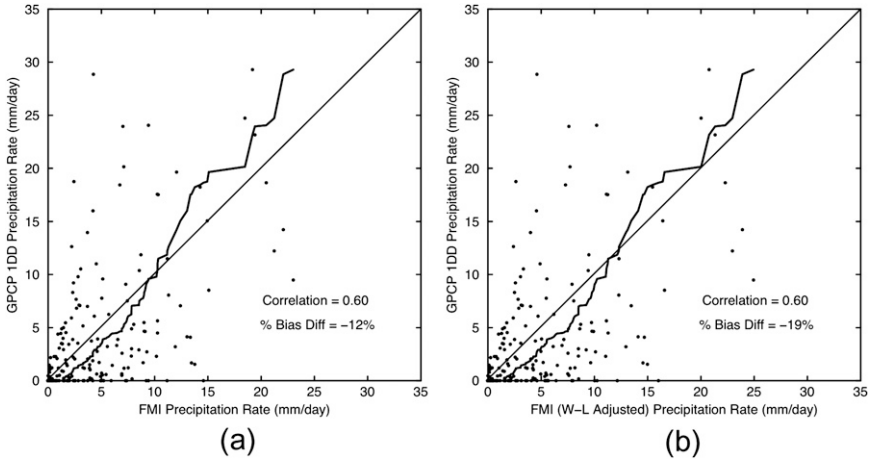

FIG. 9. Scatterplots of all daily 1° latitude × 2° longitude grid-box (a) GPCP precipitation estimates and FMI gauge observations, and (b) GPCP estimates and wind-loss-adjusted FMI gauge observations from boxes 1–8 for August 2005. The Q–Q plot for each scatterplot is provided (thick line).

biased low by 12%. The GPCP tends to underestimate precipitation at lower rates and overestimate precipitation at higher rates, as shown by the quantile–quantile plot (Q–Q plot; thick line). Figure 9b shows the same scatterplot, but using the wind-loss-adjusted FMI. Though the wind-loss adjustment is smallest in summer, the GPCP estimates are further biased low at 19%. It is possible that the bias shift from 12% to 19% may simply be the result of the limitations of the wind-loss adjustment rather than a real effect. Regardless, it is reasonable to conclude that the August GPCP has a negative bias compared to the FMI. Furthermore, there is minimal change in the shape of the Q–Q plot. Since the wind-loss adjustment is a multiplicative factor, the correlation is unchanged. It is important to note that the original Legates wind-loss adjustment is provided and used at the 2.5° resolution, so this adjustment had to be bilinearly interpolated to the 1° latitude × 2° longitude resolution for use with the daily FMI. As the original 2.5° wind-loss adjustment does vary smoothly from grid box to grid box, it is believed that no major artifacts are introduced during interpolation.

Figure 10a shows the GPCP and FMI daily scatterplot for February 2006. Note the scales along the *y* axis are different for Figs. 9a and 10a. The GPCP estimates are slightly less correlated at 0.52, but are biased high by 89%. Only at very low rates is GPCP underestimating the precipitation. Figure 10b shows the GPCP and wind-loss-adjusted FMI scatterplot. The bias in the GPCP is greatly reduced, to 10% high. The wind-loss adjustment reaches a maximum in February, which accounts for the noticeable improvement. It is clear from the scatterplot

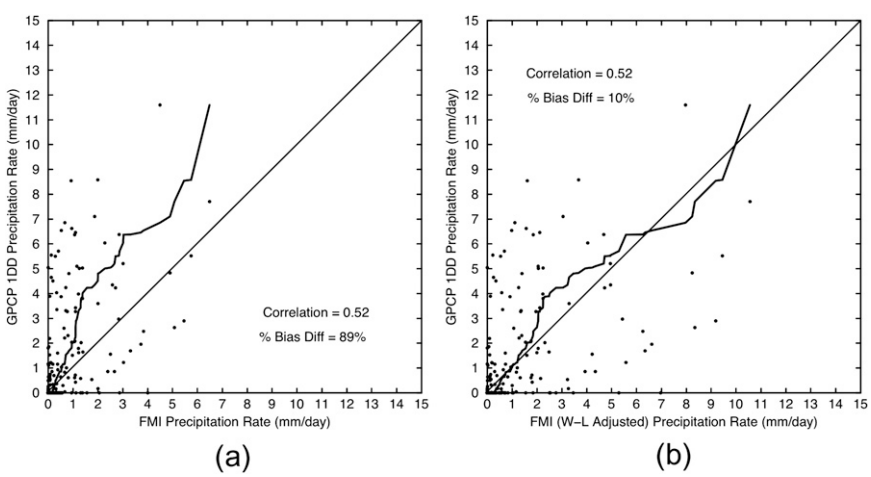

FIG. 10. As in Fig. 9, but for February 2006.

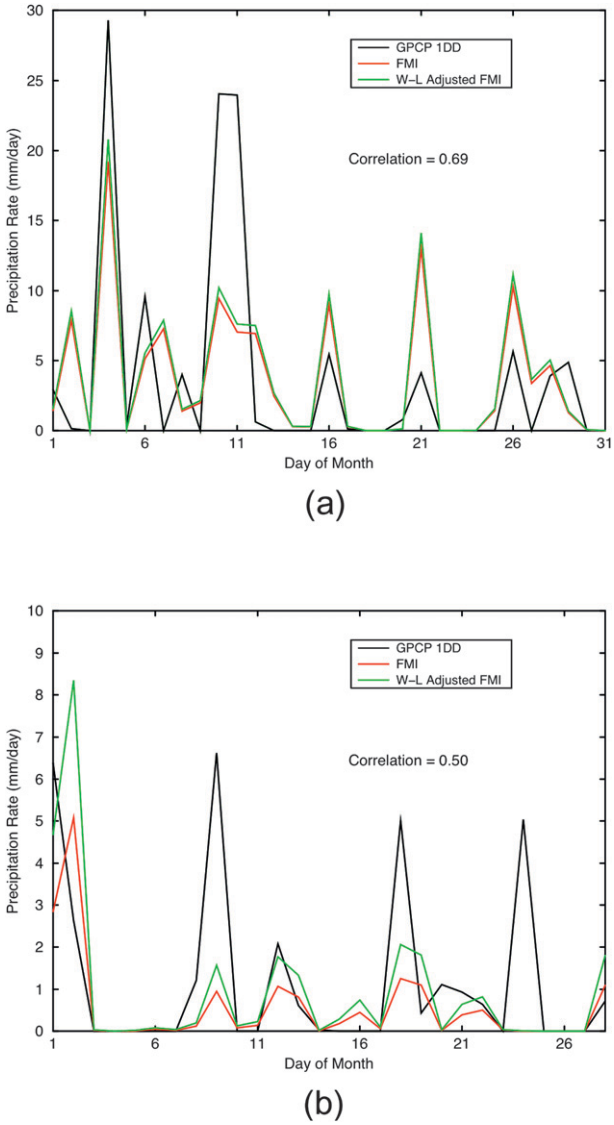

FIG. 11. Time series of daily precipitation of the GPCP (black), FMI (red), and wind-loss-adjusted FMI (green) precipitation for (a) August 2005 and (b) February 2006 for 1° latitude × 2° longitude grid box 5.

that the wind-loss adjustment is necessary. This wind-loss adjustment is implicitly included in the GPCP daily estimates through scaling with the monthly SG product, which explicitly includes the wind-loss-adjusted GPCC gauge analysis. Examination of the same analysis area for other months reveals the same general shape in the Q–Q plots: GPCP underestimates precipitation at the lowest rates (below 1 mm day^{-1}) and overestimates precipitation at higher rates. This is also seen, to some degree, for the individual 1° latitude × 2° longitude grid-box scatterplots, though the variability is much higher due to the small number of points. The underestimation by GPCP at the low end is likely due to the spatial and temporal mismatch of large-footprint satellite precipitation estimates and point gauge observations. A dense network of gauges may be more likely to measure small areas of precipitation that occur within a grid box. In contrast, the footprint size of the satellite pixel (typically measured in kilometers) may tend to alias areas of small precipitation due to detectability issues. This underestimation is more significant in August, when smaller convective cells are more dominant. In February, synoptic-scale systems dominate so there is less chance of the underestimation of precipitation by the satellite.

To assess the skill of the GPCP daily product in duplicating the day-to-day occurrences of precipitation, it is useful to show time series of daily precipitation values for a given 1° latitude × 2° longitude grid box. Figure 11a shows the daily time series of precipitation for the GPCP, FMI, and wind-loss-adjusted FMI for August 2005 for box 5 shown in Fig. 3. Though there is considerable variability from grid box to grid box in the time series, box 5 is representative of typical behavior. In general, GPCP sees the same events as the FMI with a correlation of 0.69. There are noticeable exceptions in the time series where the GPCP and FMI occurrences appear to be offset by 1 day, such as 6 and 7 August. This could be the result of the difference in the definition of a day. The GPCP day spans 0000–0000 UTC, while the FMI gauge accumulations span 0600–0600 UTC. If significant precipitation occurs within this 6-h time difference, the amount will be attributed to different days for the GPCP and FMI. This will result in an apparent lag or lead in the GPCP precipitation occurrence and affect the amount of precipitation ascribed to adjacent days. Note that the wind-loss adjustment barely changes the FMI precipitation amounts for August. The percent bias difference between the GPCP and wind-loss-adjusted FMI for box 5 is −3%, which is consistent with the results shown in Fig. 9b. Figure 11b shows the box 5 time series plot for February 2006. Note the scales on the y axis are different for Figs. 11a and 11b. The precipitation correlates reasonably well at 0.50, but the GPCP tends to overestimate the precipitation amount, even when the wind-loss adjustment, which is a maximum in February, is applied to the FMI precipitation. This behavior is also observed, to some extent, in the other red grid boxes, and is, in part, likely due to the difficulty of estimating frozen precipitation using satellite observations. The percent bias difference between the GPCP and wind-loss-adjusted FMI for box 5 is 25%, which is consistent with the results shown in Fig. 10b.

As noted previously, the FMI gauge population far exceeds the corresponding GPCC gauge population for any given grid box in the study areas. As such, it is

interesting to examine the effects of FMI gauge population on the FMI daily average precipitation and the correlations with the GPCP 1DD estimates. This was done by computing an ensemble set of 100 FMI daily time series of precipitation for box 5, with each time series using three randomly chosen FMI gauges of the available 26 and 25 gauges for August 2005 and February 2006, respectively. For August 2005, the FMI was correlated to the GPCP 1DD at 0.69 (from Fig. 11a) using the full complement of 26 gauges. The correlations for the corresponding three-gauge ensemble range from a minimum of 0.50 to a maximum of 0.79. For February 2006, the FMI was correlated to the GPCP 1DD at 0.50 (from Fig. 11b) using the full complement of 25 gauges. The correlations for the corresponding three-gauge ensemble range from a minimum of 0.35 to a maximum of 0.63. The three-gauge ensemble correlations for both August 2005 and February 2006 are reasonably contained compared to the corresponding 26- and 25-gauge correlations, respectively. In terms of bias, the 3-gauge ensemble FMI daily averages are closer to the 26- and 25-gauge FMI averages for August 2005 and February 2006, respectively, than to the corresponding 1DD averages.

It is well known that spatial and temporal averaging of precipitation will reduce noise and increase correlation (Bell et al. 1990). To quantify the effects of averaging on the correlation between the GPCP and FMI, we consider a 4° latitude × 4° longitude "master" grid box, 60°–64°N and 24°–28°E (encompassing all eight grid boxes, 1–8), and compute correlations for progressively larger spatial scales and progressively longer temporal scales. For this computation, data from all 13 Augusts and all 13 Februaries in the analysis span were used. To isolate the effect of spatial averaging, GPCP and FMI correlations are computed separately for all 1° latitude × 1° longitude, 1° latitude × 2° longitude, and 2° latitude × 2° longitude grid boxes that fall within the 4° latitude × 4° longitude "master" grid box for all Augusts and all Februaries. The result of this computation is shown in Fig. 12a. For both August and February, the correlation increases with progressively larger spatial resolution. August shows a more pronounced improvement, from 0.5 to 0.7, than February. At all spatial scales, the GPCP and FMI are more highly correlated in August than February. It is important to note the correlations in Fig. 12a for the 1° latitude × 2° longitude spatial averaging scale. These values, 0.55 for August and 0.45 for February, show that the correlations for the August 2005 and February 2006 results, shown in Figs. 9a and 10a, are consistent with the long-term average correlations.

To isolate the effects of temporal averaging, GPCP and FMI correlations are computed for all 1° latitude × 2° longitude grid boxes (within the 4° latitude × 4° longitude master grid box) averaged in time to 1, 3, 6, 10, and 30 days. The "30 day" average for February only contains 28 or 29 days. The results are shown in Fig. 12b. The GPCP and FMI correlations increase for a progressively increasing averaging time scale. As in Fig. 12a, the correlations for August are consistently higher than the correlations for February, with the 30-day averaging period being the notable exception. As concluded in previous studies (Bell et al. 1990), temporal averaging increases correlations at a faster rate than does spatial averaging.

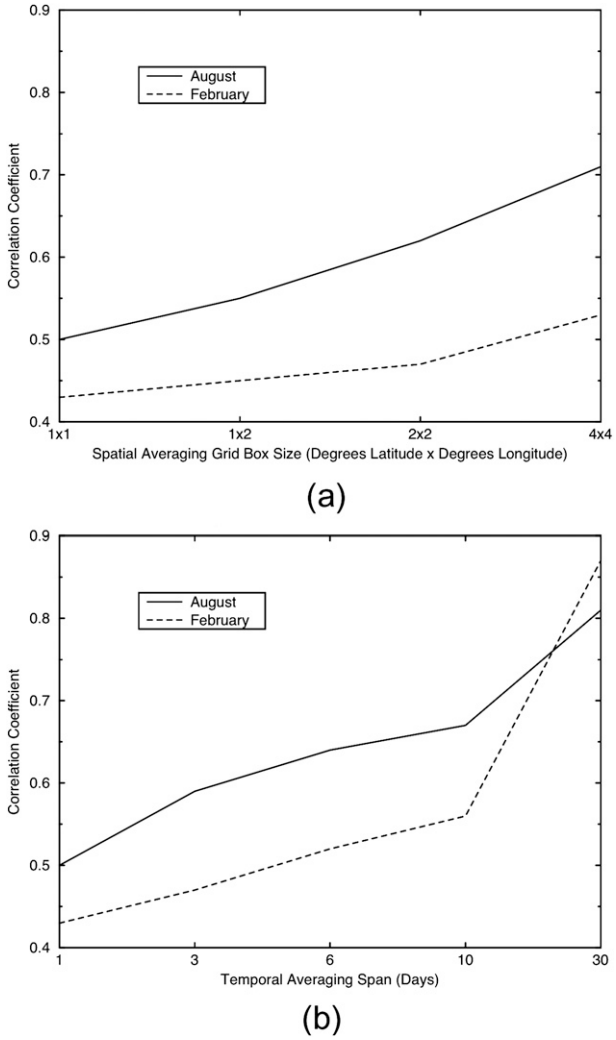

FIG. 12. Correlation coefficient between (a) the daily GPCP and FMI precipitation as a function of spatially averaging grid-box size using all Augusts (solid) and all Februarys (dashed) in the entire analysis span 1995–2007, and (b) the correlation coefficient as a function of time averaging for all Augusts (solid line) and all Februarys (dashed line) using all 1° latitude × 2° longitude grid boxes 1–8.

5. Conclusions and future work

The goal of this analysis was to compare the GPCP monthly and daily products at high latitudes with high-quality, high-density FMI gauge observations to assess the quality of the GPCP estimates. The monthly product results show the large-area, long-term-average SG duplicates the mean annual cycle of precipitation as observed by the FMI. The difference between the SG and FMI is dominated by the Legates wind-loss adjustment applied to the GPCC gauge analysis, which is heavily weighted in the SG over land. For the analysis period, the SG is biased low by 6% when compared with the wind-loss-adjusted FMI. The small low bias of the SG is likely due to the GPCC analysis scheme, which draws upon a lower gauge population and includes the influence from gauges in surrounding grid boxes. Despite the radical differences in the GPCC and FMI gauge populations, the comparison results are a testament to the overall quality of the GPCC gauge analyses when compared with dense gauge observations. These results reveal that the technique chosen for incorporating the GPCC gauge analysis into the SG, implemented in GPCP version 1 in the mid-1990s, was a judicious design choice. Like the SG, the MS also reasonably duplicates the annual cycle of FMI precipitation despite only having climatological gauge influence.

The SG and MS both capture the long-term interannual variability of precipitation as determined by the FMI. The correlation in the monthly SG anomalies is high at 0.90 or greater for all months of the year while the percent bias difference is consistently small and negative. The MS anomalies are less correlated at 0.53 or higher for all months of the year. However, MS is better correlated in the summer and fall than the winter and spring, where there exists large variability from grid box to grid box. In areas largely lacking gauge coverage, the SG is equivalent to the MS, so the MS quality should provide an estimate of a lower bound of SG quality in terms of interannual correlations.

The daily GPCP and FMI precipitation are well correlated at 0.55 for August (summer) and at a lower level, 0.45, for February (winter). These results are consistent with daily results in other studies, including BALTEX in Huffman et al. (2001). The differences between the daily GPCP and FMI can be due to a number of factors, including using a wind-loss adjustment developed on assumptions inconsistent with the FMI gauge type, interpolation of the wind-loss adjustment from 2.5°, differences in the definition of the FMI day and the GPCP day, issues with the applicability of a monthly wind-loss correction applied to the FMI at the daily scale (i.e., changes in relative frequency of snow and windiness), and assumptions concerning the rescaling of the frequency of TOVS–AIRS precipitation at the latitudes of Finland based on the precipitation frequency at 40°N (see section 2b). The daily product comparison results also show that the GPCP estimates are consistently biased low at low precipitation rates, likely the result of satellite detectability issues associated with light or small areas of precipitation or short-lived events being missed. Using the daily data, it was shown that spatial and temporal averaging improves the GPCP and FMI correlations.

The monthly comparison results show that the GPCC gauge analysis is the primary factor in determining the level of agreement between the SG and FMI since the GPCC analysis is heavily weighted over land in the SG. Several improvements to the GPCC gauge analysis have been recently implemented and are currently under consideration for use in GPCP. First, GPCC has introduced a new climatology-anomaly-based gauge analysis technique, which is designed to improve accuracy, especially over complex terrain (U. Schneider 2008, personal communication). This better gauge analysis will likely be implemented in the next version of the GPCP dataset, as it is available for the entire GPCP span from January 1979 to the present. Second, beginning in January 2007, an event-specific, gauge-by-gauge wind-loss adjustment is being distributed as part of the GPCC analyses. GPCP is still investigating how best to incorporate this significantly more accurate wind-loss adjustment. GPCP is also investigating the wind-loss adjustments developed by Yang et al. (2005), which hold promise considering the long record available in their dataset.

The skill of the daily GPCP estimates at duplicating the FMI precipitation (both liquid and solid) is quite promising, considering that the GPCP estimates at high latitudes are based primarily on statistically derived TOVS–AIRS satellite data. Further analysis needs to be performed to understand and minimize the day-to-day differences in the precipitation amounts. The success of the GPCP products at replicating the FMI precipitation at high latitudes provides strong support for pursuing future high-resolution GPM-era precipitation estimates. The analysis techniques developed here will also provide a framework within which routine comparison and assessment of GPM-era satellite estimates and rain gauge observations can be performed.

Acknowledgments. The authors acknowledge and thank the Finnish Meteorological Institute for providing the high-quality Finnish gauge dataset used in this work. The authors also acknowledge the support of Dr. W. Scott Curtis for help in generating several figures.

REFERENCES

Adler, R. F., and Coauthors, 2003: The Version 2 Global Precipitation Climatology Project (GPCP) Monthly Precipitation Analysis (1979–present). *J. Hydrometeor.,* **4,** 1147–1167.

Bell, T. L., A. Abdullah, R. L. Martin, and G. R. North, 1990: Sampling errors for satellite-derived tropical rainfall: Monte Carlo study using a space–time stochastic model. *J. Geophys. Res.,* **95,** 2195–2205.

Dinku, T., and Coauthors, 2007: Validation of satellite rainfall products over East Africa's complex topography. *Int. J. Remote Sens.,* **28,** 1503–1526.

Drebs, A., A. Nordlund, P. Karlsson, J. Helminen, and P. Rissanen, 2002: *Climatological Statistics of Finland 1971–2000* (in Finnish). Finnish Meteorological Institute, 97 pp.

Gebremichael, M., and Coauthors, 2005: A detailed evaluation of GPCP 1° daily rainfall estimates over the Mississippi River basin. *J. Appl. Meteor.,* **44,** 665–681.

Goodison, B. E., P. Y. T. Louie, and D. Yang, 1998: WMO solid precipitation measurement intercomparison: Final report. Instruments and Observing Methods Rep. 67, WMO/TD-872, World Meteorological Organization, 88 pp.

Huffman, G. J., R. F. Adler, M. Morrissey, D. T. Bolvin, S. Curtis, R. Joyce, B. McGavock, and J. Susskind, 2001: Global precipitation at one-degree daily resolution from multisatellite observations. *J. Hydrometeor.,* **2,** 36–50.

Krajewski, W. F., G. J. Ciach, J. R. McCollum, and C. Bacoti, 2000: Initial validation of the Global Precipitation Climatology Project monthly rainfall over the United States. *J. Appl. Meteor.,* **39,** 1071–1086.

Legates, D. R., 1987: *A Climatology of Global Precipitation*. Publications in Climatology, Vol. 40, University of Delaware, 85 pp.

McPhee, J., and S. A. Margulis, 2005: Validation and error characterization of the GPCP-1DD precipitation product over the contiguous United States. *J. Hydrometeor.,* **6,** 441–459.

Nicholson, S. E., and Coauthors, 2003: Validation of TRMM and other rainfall estimates with a high-density gauge dataset for West Africa. Part I: Validation of GPCC rainfall product and pre-TRMM satellite and blended products. *J. Appl. Meteor.,* **42,** 1337–1354.

Rudolf, B., 1993: Management and analysis of precipitation data on a routine basis. *Proc. Int. WMO/IAHS/ETH Symp. on Precipitation and Evaporation,* Vol. 1, Bratislava, Slovak Republic, Slovak Hydrometeorological Institute, 69–76.

——, 1996: Global Precipitation Climatology Centre activities. *GEWEX News,* Vol. 6, No. 1, International GEWEX Project Office, Silver Spring, MD, p. 5.

——, and U. Schneider, 2005: Calculation of gridded precipitation data for the global land-surface using in-situ gauge observations. *Proc. Second Workshop of the Int. Precipitation Working Group,* Monterey, CA, EUMETSAT, 231–247.

——, H. Hauschild, W. Rueth, and U. Schneider, 1994: Terrestrial precipitation analysis: operational method and required density of point measurements. *Global Precipitation and Climate Change,* M. Desbois and F. Desalmand, Eds., NATO ASI Series, Vol. 1, No. 26, Springer-Verlag, 173–186.

Serreze, M. C., A. P. Barrett, and F. Lo, 2005: Northern high-latitude precipitation as depicted by atmospheric reanalyses and satellite retrievals. *Mon. Wea. Rev.,* **133,** 3407–3430.

Shepard, D., 1968: A two-dimensional interpolation function for irregularly spaced data. *Proc. 23rd ACM National Conf.,* Princeton, NJ, Association of Computing Machinery, 517–524.

Skomorowski, P., F. Rubel, and B. Rudolf, 2001: Verification of GPCP-1DD global satellite precipitation products using MAP surface observations. *Phys. Chem. Earth,* **26,** 403–409.

Susskind, J., and J. Pfaendter, 1989: Impact of interactive physical retrievals of NWP. *Report on the Joint ECMWF/EUMETSAT Workshop on the Use of Satellite Data in Operational Weather Prediction: 1989–1993,* T. Hollingsworth, Ed., Vol. 1, ECMWF, 245–270.

——, P. Piraino, L. Rokke, T. Iredell, and A. Mehta, 1997: Characteristics of the TOVS Pathfinder Path A dataset. *Bull. Amer. Meteor. Soc.,* **78,** 1449–1472.

Willmott, C. J., C. M. Rowe, and W. D. Philpot, 1985: Small-scale climate maps: A sensitivity analysis of some common assumptions associated with grid-point interpolation and contouring. *Amer. Cartogr.,* **12,** 5–16.

Yang, D., D. Kane, Z. Zhang, D. Legates, and B. Goodison, 2005: Bias corrections of long-term (1973–2004) daily precipitation data over the northern regions. *Geophys. Res. Lett.,* **32,** L15901, doi:10.1029/2005GL024057.